THE JOURNAL OF PHYSICAL CHEMISTRY C

Article

pubs.acs.org/JPCC

Preparation and Spectroscopic Properties of Monolayer-Protected Silver Nanoclusters

Mostafa Farrag,[†] Martin Thämer,[†] Martin Tschurl,*[,†] Thomas Bürgi,[‡] and Ueli Heiz[†]

[†]Lehrstuhl für Physikalische Chemie, Technische Universität München, Lichtenbergstrasse 4, 85748 Garching, Germany

[‡]Département de Chimie Physique, Faculté Des Sciences, University of Geneva, Quai Ernest-Ansermet 30, 1211 Genève 4, Switzerland

Supporting Information

ABSTRACT: Silver nanoclusters protected by 2-phenylethanethiol (**1**), 4-fluorothiophenol (**2**), and L-glutathione (**3**) ligands were successfully synthesized. The optical properties of the prepared silver nanoclusters were studied. The absorption signal of Ag@SCH_2CH_2Ph in toluene can be found at 469 nm, and Ag@SPhF in THF shows two absorption bands at 395 and 462 nm. Ag@SG in water absorbs at 478 nm. Mie theory in combination with the Drude model clearly indicates the peaks in the spectra originate from plasmonic transitions. In addition, the damping constant as well as the dielectric constant of the surrounding medium was determined. In addition, the CD spectra of silver nanoclusters protected by the three ligands (**1**−**3**) were also studied. As expected, only the clusters of type **3** gave rise to chiroptical activity across the visible and near-ultraviolet regions. The location and strength of the optical activity suggest an electronic structure of the metal that is highly sensitive to the chiral environment imposed by the glutathione ligand. The morphology and size of the prepared nanoclusters were analyzed by using transmission electron microscopy (TEM). TEM analysis showed that the particles of all three types of silver clusters were small than 5 nm, with an average size of around 2 nm. The analysis of the FTIR spectra elucidated the structural properties of the ligands binding to the nanoclusters. By comparing the IR absorption spectra of pure ligands with those of the protected silver nanoclusters, the disappearance of the S−H vibrational band (2535−2564 cm^{-1}) in the protected silver nanoclusters confirmed the anchoring of ligands to the cluster surface through the sulfur atom. By elemental analysis and thermogravimetric analysis, the Ag/S ratio and, hence, the number of ligands surrounding a Ag atom could be determined.

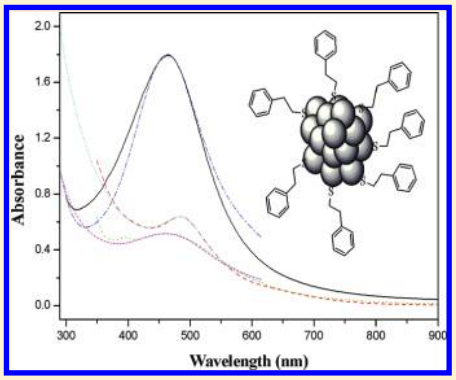

INTRODUCTION

Noble metal clusters have stimulated major research interest in recent years.[1−3] Thiolate monolayer-protected clusters (MPCs) consist of a metallic core that is surrounded by ligands that stabilize the clusters and can subsequently being modified. In addition, it is possible to dissolve, dry, and redissolve these types of nanoparticles without suffering from degradation.[4] Usually, ligand-protected clusters possess properties that make them accessible to synthetic altering, which is essential for various applications.[5−10] The optical and electronic properties of the metal nanoclusters (MNCs) have made them suitable for many applications in various fields of science, such as bioscience,[5−7] nanophotonics,[8] and nanoelectronics.[9,10] Therefore, NPs have attracted large research efforts, and their properties depend strongly on the particle size[11−13] and shape,[14,15] the surrounding medium,[16] and the aggregation state.[15]

Concerning their optical properties, the dominating feature in the optical spectra of silver nanoclusters is usually the surface plasmon resonance, which can be described by the classical Mie theory. The resonance position and the peak width depend on many factors and give insight into several physical properties of the MPCs. For small silver clusters (<10 nm), the Mie theory predicts almost no influence of the cluster size on the position of the resonance, which is located around 350 nm for small spherical Ag clusters in vacuum (calculated from Mie theory). However, already small changes in the electronic properties of the surrounding medium of the cluster lead to strong shifts of the peak.

On the basis of the properties of these shifts, the electronic interaction between the cluster and its surroundings can be derived. Since MPCs consist of a metallic core covered by ligands, the surroundings of the cluster is governed by these ligands, and therefore, additional information about the metal−ligand bond can be obtained from these shifts. The cluster size in that region of a couple of nanometers has mainly an influence on the peak width caused by the free mean path effect[17] of the free electrons inside the cluster. Here, the width increases with decreasing cluster size due to additional scattering processes of the oscillating electrons at the cluster surface.

Received: October 31, 2011
Revised: March 2, 2012
Published: March 5, 2012

   dx.doi.org/10.1021/jp210453v | J. Phys. Chem. C 2012, 116, 8034−8043

Another effect that leads to a broadening of the surface plasmon is the so-called electron spill out effect.[18] This effect can be highly enhanced by delocalization of the conduction electrons over the ligands. However, the influence of ligands on the electron spill out is not yet fully understood.

For very small Ag clusters (<8 atoms) the concept of a plasmon does not hold anymore because the energy bands of the cluster split into discrete energy levels. Here, the broad plasmon absorption band is predicted to split into sharp molecular-like transitions;[19] however, the spectra of the Ag clusters used in this work can be treated using the classical description of surface plasmons because their size is in the nanometer scale.

It is well-known that metal surfaces can exhibit an intrinsically chiral structure.[20] Furthermore, chirality can be transferred to achiral metal surfaces by the adsorption of chiral molecules.[21,22] Similarly, metal NPs can exhibit chirality, which can be found by their optical activity of the electronic transitions that are metal-based; however, transfer of chirality from the adsorbate to the metal surface strongly depends on the structure of the former. Chiroptical techniques such as electronic circular dichroism (CD) and vibrational circular dichroism (VCD)[23] are valuable tools to elucidate this transfer of chirality from the ligand to the nanoparticles. Due to their organic shell, monolayer-protected AgNPs can be dissolved in various solvents and are thus amenable to these techniques.

A well-established route to prepare solution phase metal clusters is to use strong ligands (such as thiols) to protect the clusters and effect size control.[24−29] Among the noble metals, gold clusters are being extensively studied because of their chemical stability and relative ease of preparation, even under ambient conditions. Some well-defined, monodisperse Au_n nanoclusters have been reported, and their exact formulas have been determined by electrospray ionization mass spectrometry analysis (ESI-MS).[25−28] Work on understanding the electronic and atomic structures of this class of clusters has accelerated, including the complete structural determination of clusters consisting of 25, 38, and 102 gold atoms.[25−28]

Both Au and Ag are noble, free electron metals and have almost identical bulk lattice constants. On the basis of these similarities, Ag could be expected to follow the same shell closing rules as Au;[29] however, thus far, the shell closing rules for Ag remain unexplored. In the present study, we show that it is possible to synthesize Ag clusters that are protected by different ligands, which opens the door to study these important MNC in the future in more detail.

In this article, we report the synthesis of new silver nanoclusters protected by 2-phenylethanethiol (**1**) (Scheme 1), 4-fluorothiophenol (**2**), and L-glutathione (**3**) ligands by different protocols (see the Experimental Section). For the sake of characterization, the optical properties of these silver nanoclusters are studied by UV−vis spectroscopy and Fourier transform infrared spectroscopy (FTIR). The size and composition of AgNCs were assessed by thermogravimetric analysis (TGA), elemental analysis, and transmission electron microscopy (TEM).

EXPERIMENTAL SECTION

Chemicals. Silver nitrate ($AgNO_3$, ≥99% metals basis, Aldrich), sodium borohydride (99% metals basis, Aldrich), 2-phenylethanethiol (2-PET, 99%, Aldrich), 4-fluorothiophenol (4-FTP, 99%, Aldrich), and glutathione (γ-L-glutamyl-L-cysteinylglycine, γ-Glu-Cys-Gly, L-GSH) reduced (98%) were used for synthesizing the ligand-protected nanoparticles (for the chemical structure of the used ligands, see Scheme 1). The solvents used were tetrahydrofuran (THF, HPLC grade, ≥99.9%, Aldrich), toluene (HPLC grade, ≥99.9%, Aldrich), ethanol (HPLC grade, Aldrich), and methanol (HPLC grade, Aldrich). All chemicals were used as received. Deionized water was purified by a Millipore Milli-Q water system to obtain Milli-Q water (resistivity 18.2 MΩ x cm). All glassware was thoroughly cleaned with aqua regia (HCl/HNO_3 = 3:1 v/v), rinsed with Milli-Q water, and then dried in an oven prior to use.

Scheme 1. The Ligands Used for Protecting the Clusters: 2-PET, 4-FTP, and L-Glutathione

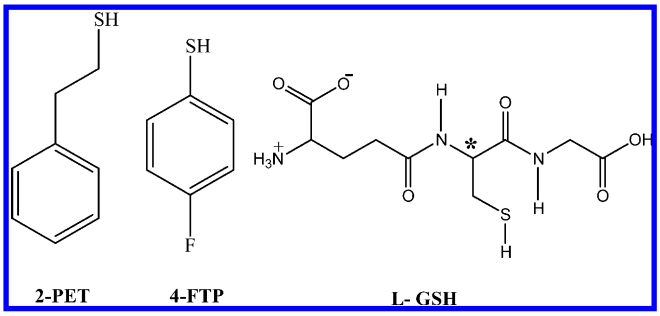

Preparation of Ag@SCH_2CH_2Ph Nanoclusters. The silver salt ($AgNO_3$, 265 mg, 1.56 mmol) was dissolved in 5.3 mL of Milli-Q water and was added afterward to 1.25 mL (9.33 mmol) of $PhCH_2CH_2SH$ (2-PET) in 100 mL of methanol under ice-cold conditions with vigorous stirring (20 min). Silver was reduced to the zero-valence state by dropwise addition of freshly prepared aqueous $NaBH_4$ solution (590 mg, 15.6 mmol in 25 mL of ice-cold Milli-Q water) and stirring vigorously (∼1100 rpm). The color of solution changed to dark brown, indicating the formation of nanomaterial. The reaction mixture was stirred for another 1 h. The resulting precipitate was then collected through centrifugal precipitation and repeatedly washed with methanol to remove the unreacted material (e.g., unreacted ligands and Ag(I) thiolate complexes). Finally, the Ag@SCH_2CH_2Ph (**1**) nanocluster precipitate was dried and collected as a dark brown powder (Scheme 2).

Preparation of Ag@SPhF Nanoclusters. Thirty milligrams of silver nitrate (0.176 mmol) was dissolved in 18 mL of THF and stirred for 5 min. 4-Fluorothiophenol (4FTP) (38 μL, 0.357 mmol) was added to that solution and the resulting solution was stirred for another 15 min. During this time, the color of the solution changed from colorless to yellow, indicating the formation of Ag(I) thiolate complexes. A 71.5 mL THF solution of $NaBH_4$ (27 mg, 0.715 mmol) that had been stirred previously for a total of 30 min was then added slowly to the reaction vessel. A change in the the color of the solution from yellow to orange to brown and, finally, to dark brown over a period of 5 min was observed. The reaction mixture was left to stir for an additional 3 h, after which 11.5 mL of Milli-Q water was added. After stirring for another minute, the reaction vessel was then stored in a freezer (at −4 °C) for 7 days. Since the final product is soluble in THF, the THF layer was separated from the frozen aqueous layer by decantation. At this stage of the preparation, the solution was found to remain stable under refrigeration or even at room temperature for several months in the dark. At all reaction stages, the formation and the stability of the samples were checked using UV−vis spectroscopy due to the characteristic

dx.doi.org/10.1021/jp210453v | J. Phys. Chem. C 2012, 116, 8034−8043

Scheme 2. Preparation Steps of $Ag@SCH_2H_2Ph$[a]

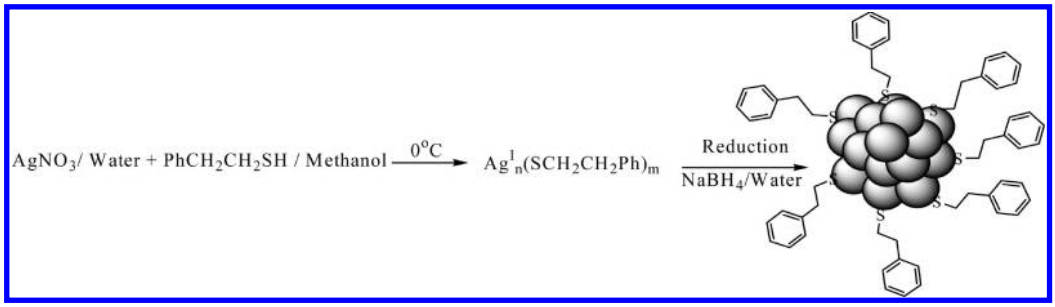

[a]A 1.56 mmol portion of $AgNO_3$ in water and 9.33 mmol of $PhCH_2CH_2SH$ in methanol were stirred under ice-cold conditions, then 15.6 mmol of $NaBH_4$ was dropwise added with vigorous stirring. The color of the solution changed to dark brown, indicating the formation of nanomaterial. The reaction mixture was stirred for 1 h. The dark brown precipitate is $Ag@SCH_2CH_2Ph$ (**1**) nanoclusters.

absorption bands of the clusters that will vanish if the sample decomposes.

For the application of thermogravimetric analysis, elemental analysis, atomic absorption spectrometry, and transmission electron spectroscopy, a solid sample is needed. Therefore, the THF solution of the clusters was concentrated under vacuum at room temperature. Afterward, cold water was added, and the precipitate was then collected and dried under vacuum to obtain a solid sample of pure Ag@SPhF (**2**) nanoclusters.

Preparation of Ag@SG Clusters. A 94 mg portion silver nitrate (0.87 mmol) was dissolved in 10 mL of Milli-Q water, and 300 mg of L-glutathione (0.97 mmol) was added afterward. The solution was then stirred vigorously at room temperature for 30 min. The resulting solution was cooled to 0 °C in an ice bath over a period of 20 min, and a freshly prepared aqueous solution of $NaBH_4$ (378 mg, dissolved in 20 mL of ice-cold Milli-Q water) was added under vigorous stirring conditions (~1100 rpm). The reaction was allowed to proceed under constant stirring for 2 h. Following that, 25 mL of ethanol was added to precipitate the clusters. After filtration, the brown precipitate of Ag@SG (**3**) nanoclusters was washed with excess ethanol.

Instrumentation and Characterization. To obtain the UV–vis absorption spectra of type **1**, **2**, and **3** nanoclusters, solutions of ~1 mg/mL were prepared in toluene, tetrahydrofuran, and water, respectively. The spectra of all the solutions were recorded at ambient temperature from 190 to 1100 nm with a single-beam spectrophotometer (Analytik Jena, Specord 40). CD spectra of nanoclusters of type **1**–**3** were measured with a Jasco J-710 spectropolarimeter using a quartz cell of 1 cm path length and solutions of about the same concentration and using the previously described solvents. Infrared spectra of 2-phenylethanethiol and 4-fluorothiophenol as well as $Ag@SCH_2CH_2Ph$ (**1**) and Ag@SPhF (**2**) nanoclusters were obtained using an FTIR spectrometer (Nicolet 380, resolution: < 0.9 cm^{-1}, transmission mode). Each spectrum was obtained by accumulating 200 scans. The infrared spectra of L-glutathione ligand and Ag@SG (**3**) nanoclusters were recorded with a FTIR spectrometer (Vertex 70, Bruker, resolution: 2 cm^{-1}, transmission mode). Again, a spectrum was obtained by accumulating 200 scans. All the samples were measured using a single-reflection diamond ATR accessory, which was installed into the Vertex FTIR spectrometer.

Thermal gravimetric analysis (~ 2 mg sample tested) was conducted in a N_2 atmosphere (flow rate ~ 50 mL/min) with a TG/DAT Q5000 IR analyzer (TA Instruments, Inc.). All measurements were performed with a heating rate of 10 °C/min, starting from room temperature and ranging up to 900 °C. Analysis of C, S, N, and H content was performed by an elemental analyzer (Euro EA) that allowed controlled combustion of the samples with subsequent chromatographic separation and the detection of the as-separated species with a TCD detector. The amount of Ag was analyzed by a fast sequential atomic absorption spectrometer (Varian AA 280 FS) using a Ag lamp as light source. AgNCs were dissolved in aqua regia, and the solution was then evaporated completely. The sample was redissolved in 10% HCl. For calibration, Ag solutions of different concentrations were prepared using the standard matrix.

Samples were prepared for TEM measurements by the production of 1–2 mg/mL nanocluster solutions. These solutions were obtained by dissolving the nanocluster material in solvents with the aid of sonication. For clusters of type **1** and **2**, water and toluene were used as solvents, respectively, and for the clusters of type **3**, a mixture of water/ethanol, 1:1, was used. The samples were prepared for analysis by casting a droplet of MPC solution onto carbon-coated copper grids. The solvent was then allowed to evaporate slowly. TEM images were obtained at a magnification of 100 000 for types **1** and **3** clusters and a magnification of 150 000 for type **2** clusters with a JEOL 100CX electron microscope operating at an acceleration voltage of 100 kV. The images were then analyzed using Image J software (version 1.44).

■ RESULTS AND DISCUSSION

After having successfully synthesized Ag MPCs they were characterized with respect to their chemical composition, the ligand–metal bonding, their size, and their stability. Furthermore, in this section, we present and discuss the optical spectra and show the CD spectra of all three types of clusters.

Chemical Composition of Ag MPCs. One way of deducing the exact number of silver atoms and thiolate ligands of the particle is to determine the Ag/S ratio. This ratio can be obtained by performing elemental analysis or thermogravimetric analysis. In both methods, the organic content is determined, and from that, the Ag/S atomic ratio can be calculated.[30]

TGA analysis shows that the organic weight loss of the 2-PET- and 4-FTP-protected silver nanoclusters is 48.95% (wt) from 224 to 246 °C and 35.85% from 201 to 225 °C (Figure 1), respectively. Therefore, the silver content of $Ag@SCH_2CH_2Ph$ is calculated as 51.05% and for Ag@SPhF, as 64.15% (for a complete summary of the elemental composition

dx.doi.org/10.1021/jp210453v | J. Phys. Chem. C 2012, 116, 8034–8043

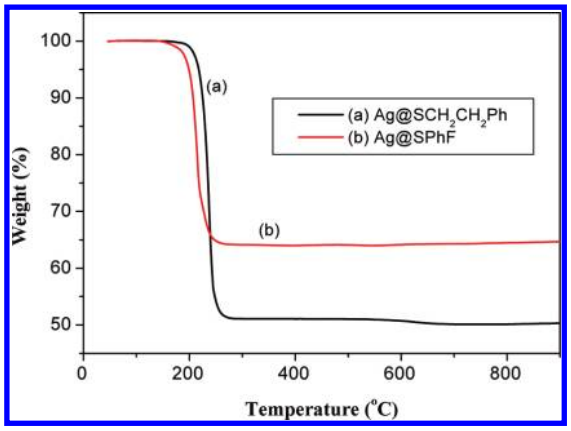

Figure 1. Theromgravimetric analysis of $Ag@SCH_2CH_2Ph$ and Ag@SPhF nanoclusters. For $Ag@SCH_2CH_2Ph$ nanoclusters (a), the percentage of the organic layer is 48.95%, and the rest is silver metal (51.05%). The decomposition of the clusters starts at 224 °C. Ag@SPhF nanoclusters (curve b) consist of an organic layer, which is 35.85% of their total mass. Again, the rest (64.15%) is only silver metal. These clusters start to decompose at 201.5 °C.

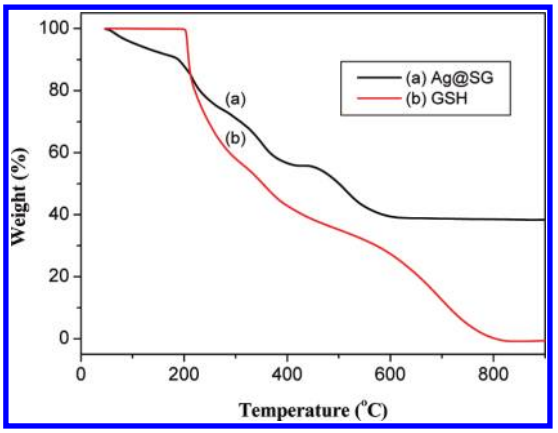

Figure 2. TGA of Ag@SG nanoclusters (curve a) and glutathione ligand (curve b). (a) Ag@SG shows four steps of mass loss upon heating from 40 to 900 °C. In the first step (40−180 °C), involves adsorbed water molecules (9.16%). The total mass loss during the remaining three steps from 180 to 900 °C amounts to 51.74% (16.71%, 18.09%, and 16.94%, respectively). (b) The first step (200.50−299.35 °C) amounts to 41.74%, the second step (299.35−451.94 °C) amounts to 19.37%, and the third step from 451.94 to 819.51 °C (38.90%) completes the destruction of glutathione.

of these two clusters, see Tables S1 and S2 in the Supporting Information). The 48.95% (wt), and 35.85% loss converts to an Ag/S atomic ratio of 1/0.75 and 1/0.47, respectively. This composition is further supported by the elemental analysis of the $Ag@SCH_2CH_2Ph$ and Ag@SPhF nanoclusters, which show that the organic content of these clusters consists of 34.28% C, 3.28% H, 11.49% S, and 20.41% C and 1.19% H, 8.95% S, 5.41% F, respectively (see again Tables S1 and S2 in the Supporting Information). Thus, the molar ratio of C/H/S in nanoclusters of type **1** is 7.96:9.08:1, which equals the molecular formula of phenylethylthiolate (C_8H_9S). Looking at the type **2** nanoclusters, a molar ratio of C/H/F/S = 6.08:4.23:1.01:1 is found, which is also in very good agreement with the chemical formula of 4-fluorothiophenolate (C_6H_4FS). In addition, by using atomic absorption spectroscopy, the percentage of Ag was directly obtained. It was found to be 50.95% for clusters of type **1** and 64.04% for clusters of type **2** (see Tables S1 and S2 in the Supporting Information), thus confirming composition obtained from thermogravimetric analysis.

In contrast to nanoclusters of types **1** and **2**, which show only one step of mass loss in their thermogravimetric curve, four steps can be found when heating Ag@SG (**3**) up to 900 °C (Figure 2a). In the first step (from 40 to 180 °C), the mass loss (9.16%) is caused by the evaporation of adsorbed water molecules. This assignment is based on the comparison with the curve of the ligand only, which shows no mass loss until 200 °C (Figure 2b). This phenomenon can also be found in the thermoanalysis of gold nanoparticles[31,32] protected by mercaptosuccinic acid.[31]

Concerning the other steps, they might be interpreted analogously to the TG curve of pure glutathione: In the thermoanaylsis of the bare ligand, three steps of decomposition can be found during heating from 40 to 900 °C (Figure 2b). The first step (200−300 °C) amounts to a loss of 41.74% of the total mass, corresponding to the hydrolysis of glutathione to hydrolyzed glutathione,[31] which equals 129 Da (the theoretical amount of this part is 42%). This is consistent with the work of Teranishi et al. who found that $Au_{25}(SG)_{18}$ shows the same weight loss plus one hydrogen atom (130 Da) in ESI mass spectroscopy.[27a]

The second step (300 − 452 °C) amounts to a mass loss of 19.37%, and the third step from 452 to 820 °C (38.90% mass loss) completes the destruction of glutathione. The total mass loss of these three steps is 100%, showing complete removal upon heating.

Note that the sum of the total mass loss of the last three steps of the TG curve of Ag@SG (**3**) equals 51.74%. This value is much less than that of the total organic content (69.09%) that is obtained from elemental analysis (see Table S3 in the Supporting Information). Therefore, it can be concluded that not all of fragments of the ligands are evaporated, and some of the organic residues still remain on the metal compound. Consequently, TG analysis overestimates the percentage of the Ag content (39.10%) in comparison with atomic absorption spectroscopy analysis 30.91% (see Table S3 in the Supporting Information).

Finally, the TGA residue was also investigated with atomic absorption spectrometry and elemental analysis. Although the first method showed the amount of Ag to be only 44.7% (instead of 100%), the latter method determined the composition of the organic species to be 22.75% C, 1.22% H, 1.17% N, 4.91% S, with the remaining amount being oxygen. These measurements independently confirm the ligand not to be evaporated into the gas phase entirely. The Ag/S atomic ratio for Ag@SG (**3**) is 1/0.76, as obtained from elemental analysis. The elemental analysis further shows that the Ag nanocluster of type **3** contains 26.13% C, 3.95% H, 7.01% S, 8.96% N, and 23.04% O (Table S3 in the Supporting Information). Thus, the molar ratio of C/H/N/O/S is found to be 9.95:16.28:2.92:5.99:1, which is in very good agreement to the molecular formula of glutathione ($C_{10}H_{16}N_3O_6S$), after subtracting the percentage of hydrogen (0.36%) and oxygen (2.11%) originating from adsorbed water (9.16%).

To summarize this section, clusters of type **1** and **2** consist of silver atoms and the ligand only. The TG curves of these species consist of only one step, indicating that the ligand boils off the cluster in just one process. Neither sample shows any impurities of water, and there are no residues left on the clusters after heating them to 900 °C. In case of type **1**

dx.doi.org/10.1021/jp210453v | J. Phys. Chem. C 2012, 116, 8034−8043

nanoclusters, it is found that the molecular formula equals $Ag_{4n}L_{3n}$; in clusters of type **2**, the formula is found to be $Ag_{2n}L_n$. However, the behavior of type **3** nanoclusters is completely different. They are hygroscopic (indicated by the loss of water when starting the heat-up process), and like the bare ligand, the organic species decomposes when heated. Furthermore, it is not possible to evaporate the entire organic compound, so even after heating the clusters to 900 °C, residues of the ligands stick to the clusters. Like at nanoclusters of type **1**, again, the chemical formula of the species is $Ag_{4n}L_{3n}$ for type **3** clusters.

Characterization of Ligand–Metal Bonding. To characterize the bonding between the ligands and the cluster, FT-IR spectroscopy was used to observe changes in the vibrational spectra of the ligands upon adsorption. Figure 3 shows the vibrational spectrum of 2-phenylethanethiol (2-PET) with the antisymmertic (d^-) CH_2 stretching band at 2932 cm^{-1}, the symmetric (d^+) CH_2 stretching modes at 2851 cm^{-1},[33,34] and the C–H aromatic stretching bands in the range of 3025–3085 cm^{-1}. Also observed in the spectrum is the vibrational band at 2535–2564 cm^{-1} typical for the S–H excitation. As expected, this band completely disappears upon formation of the Ag@SCH_2CH_2Ph nanoclusters (**1**), as depicted in the inset of Figure 3. This indicates the ligands are anchored to the cluster via the sulfur atom.[35,36]

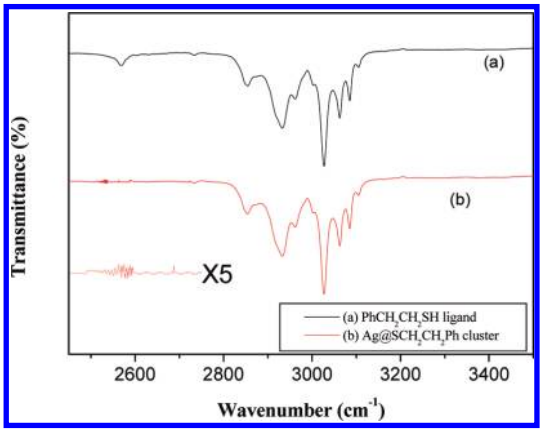

Figure 3. FTIR spectra of 2-phenylethanethiol $PhCH_2CH_2SH$ (a) and Ag@SCH_2CH_2Ph nanoclusters with inset of Ag@SCH_2CH_2Ph nanoclusters (× 5) (b). The spectra show that the band around 2560 cm^{-1} disappears in the spectrum of the cluster with respect to that of the bare ligand. This band can be assigned to the S–H stretching frequency, and its disappearance clearly indicates that the ligand is bound to the cluster via the sulfur atom. Since the spectrum of the clusters otherwise stays more or less unaltered, it can be concluded that no further changes happened to the ligand.

As expected, this observation is also true for the other two Ag-MPCs. The corresponding spectra are given in the Supporting Information (Figures S1–2), and the results can be summarized as follows: The presence of 4-FTP in Ag@SPhF nanoclusters (**2**) is manifested by C–H aromatic stretching bands in the range of 3025–3085 cm^{-1}; aromatic ring stretch moieties in the range of 1476–1695 cm^{-1}; and the C–F stretching band (symmetric) at ∼1250 cm^{-1} (Supporting Information Figure S1b), which occurs at the same position as in the case of the parent 4-florothiophenol ligand (Supporting Information Figure S1a). The presence of L-GSH in Ag@SG nanoclusters (**3**) is confirmed by several bands (Supporting Information Figure S2b), such as the N–H stretching at 3310–3500 cm^{-1}. Furthermore, the hydrogen in the carboxylic acid is featured by the broad carboxylic acid O–H stretching band centered near 3000 cm^{-1}, which is superimposed on the C–H stretching bands (2800–3100 cm^{-1}).[31] The carbonyl group of the carboxylic group (C═O–OH) shows a characteristic band at ∼1723 cm^{-1}. The C–O stretching vibration can be identified by the bands at 1315 and 1425 cm^{-1}. The peak at 937 cm^{-1} (in the range 875–960 cm^{-1}) is characteristic of the out-of-plane O–H bending mode, which occurs at nearly the same position as in the case of the parent glutathione ligand (Supporting Information Figure S2a). These results clearly point toward the stabilization of the metal cluster through sulfur bonds but otherwise support an unaltered ligand structure.

Cluster Size of the Ag-MPCs. There are, in general, several ways to determine the size of monolayer-protected metal clusters. The easiest method that can be used is UV–vis spectroscopy, since the optical properties of the metal particles change with their size. As we discuss below, the position and the width of the plasmon peak allows drawing some conclusions about cluster size; however, in contrast to bare metal clusters, the ligand has a strong effect on the plasmon peak, as well, and in the case of MPC the optical spectra, are

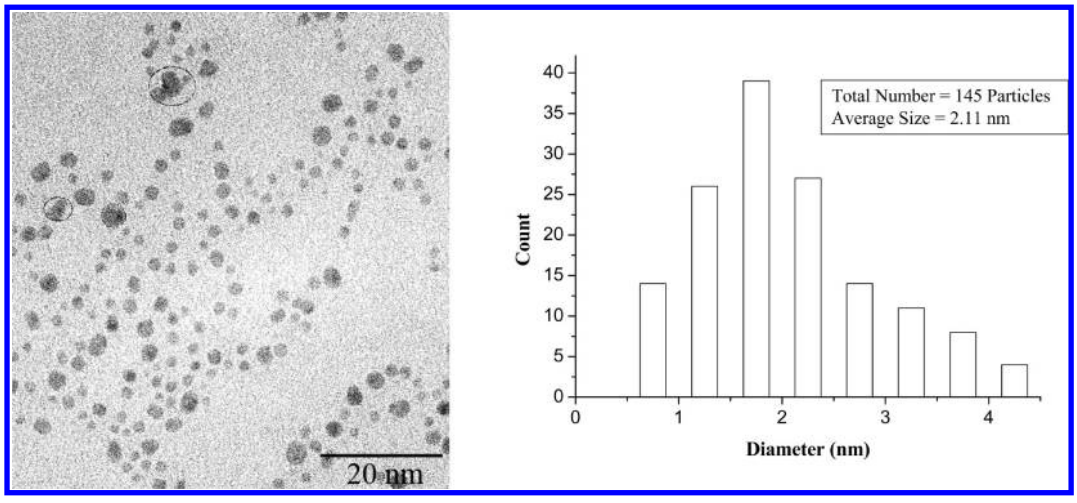

Figure 4. TEM image and size distribution of Ag@SCH_2CH_2Ph nanoclusters. A total of 145 particles were used to get the statistics for the size distribution of the clusters, which is shown on the left-hand side of the figure. The average size of the clusters was 2.11 nm.

dx.doi.org/10.1021/jp210453v | J. Phys. Chem. C 2012, 116, 8034–8043

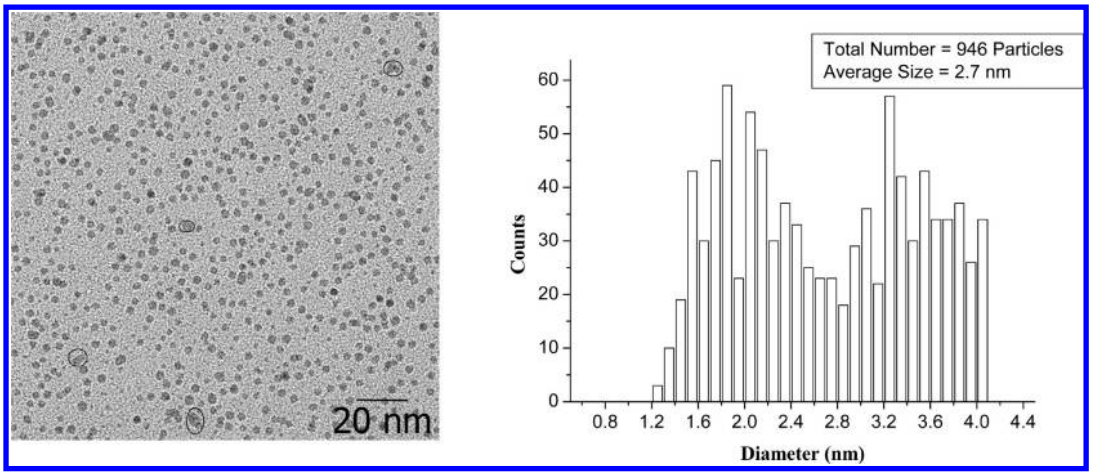

Figure 5. TEM image and size distribution of Ag@SPhF nanoclusters. These clusters show an average size of 2.7 nm (946 particles were used to obtain this average size); however, their distribution is not a Gaussian one, and it seems that it consists of two maxima.

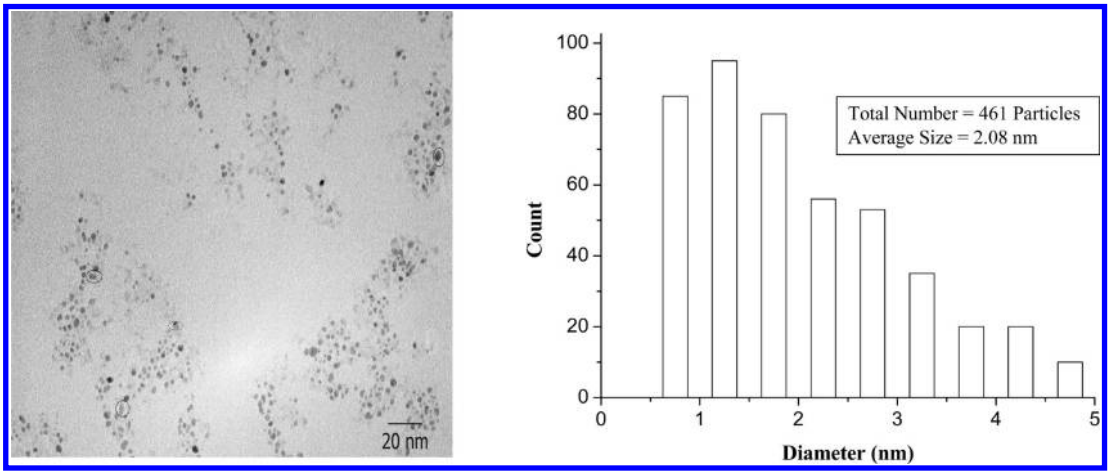

Figure 6. TEM image and size distribution of Ag@SG nanoclusters. Ag@SG nanoclusters consist of an average size of 2.08 nm (461 particles were used to obtain this average size).

rather helpful in determining the electronic properties of the cluster rather than deducing the size of the nanoparticles.

Another possibility is to use mass spectrometry. However, since the particles are rather large, a large mass range must be used, in particular, since the clusters do not form multiply charged ions easily.[37] In the case of Au-MPCs, it was shown[26a,c] that it is possible to obtain mass spectra with no or very little fragmentation; however, such experiments are not standard, and we did not characterize our samples by mass spectrometry.

Therefore, our method of choice was to use transmission electron microscopy. For clusters larger than 1 nm, TEM is in particular a very powerful technique. Because of the large scattering cross section of the metal atoms, such systems show a strong contrast in the TEM image. However, since the sample has to be deposited on a surface for performing TEM measurement, on this surface, migration and, finally, coalescence of the particle may occur. In this case, the measurement erroneously would suggest larger particle sizes than in reality. However, since our silver clusters are protected by ligands, this coalescence can more or less be ruled out, and just a sticking of the particle to each other might occur while they still possess an intact ligand shell (this effect will be called aggregation). As mentioned previously, conventional TEM is a very powerful technique for recording particles with a diameter larger than 1 nm; however, with smaller particles, the contrast becomes very weak so that very small particles might not be detected. Therefore, the statistics derived from the TEM images shown below give an upper limit of the cluster size.

Concerning the statistics, the center-of-particle and the particle size distribution were evaluated using the image processing program Image J developed at the National Institutes of Health. The average diameter of the MPCs represents the Feret's diameter and was determined in two different ways, in each case assuming a spherical shape: one value represents the average diameter of all MPCs, and the other one is received from a Gaussian fit of the frequency distribution, assuming that the larger diameters result from agglomerated MPCs.

Figures 4−6 depict typical TEM images together with size distribution histograms of the different MPCs of type **1**−**3**. In general, individual spherical nanoparticles can be seen for all the samples.[38] As mentioned above, larger core sizes are more easily visualized than small cores and can, as a consequence, become overcounted.[39] In addition, some of the MPCs in both TEM images have cores that are substantially nonspherical, and the differences in contrast within the same core indicate that they are composed of multiple grains. We attribute these nonspherical cores to the result of aggregation, in which two or a few smaller cores stick together (marked by circles), and therefore, we did not use it in the statistics. Using this setting,

dx.doi.org/10.1021/jp210453v | J. Phys. Chem. C 2012, 116, 8034−8043

we obtained average sizes of 2.11, 2.7, and 2.08 nm for the dispersed particles by taking the average of 145, 946, and 461 particles for Ag@SCH$_2$CH$_2$Ph, Ag@SPhF, and Ag@SG nanoclusters, respectively. In addition, Ag@SPhF clusters show a bimodal distribution, probably originating from two different mechanisms during cluster formation.

UV−vis Spectra of the Synthesized Clusters. Figure 7 shows the absorption spectra of 2-PET- (**1**), 4-FTP- (**2**), and

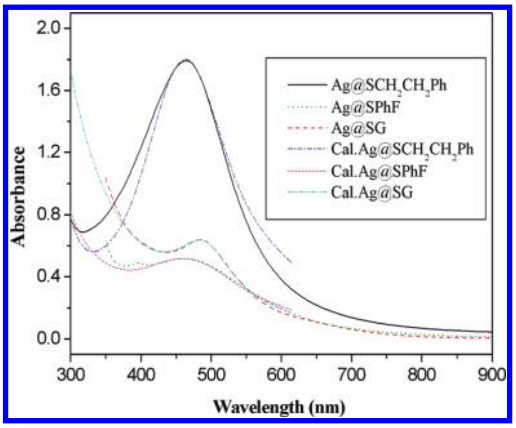

Figure 7. UV−vis absorption spectrum of all three types of nanoclusters (**1**−**3**) and simulation of the plasmon resonance. All three spectra where fitted by a function obtained by using the Mie theory[41] and the Drude model.[43] By varying the parameter for the damping constant ($\Gamma_{cluster}$) and the dielectric constant of the environment of the cluster (ε_m), it can be shown that in all three cases, there is a strong spill-out effect of the electron density to the ligand, which is strongest in the case of Ag@SPhF.

GSH- (**3**) protected silver nanoclusters. Although 2-PET-protected silver nanoclusters (**1**) in toluene exhibit a broad peak around 469 nm, FPhS-protected silver nanoclusters (**2**) in THF shows two absorption bands: one broad peak at 462 nm and a small absorption peak at 395 nm. GS-protected silver nanoclusters (**3**) in water absorb at 478 nm. All of the clusters exhibit broad peaks in the visible to near-UV region. Kitaev et al. have prepared monolayer-protected silver nanoclusters with a mixture of two ligands, captopril and glutathione, using a multistage cyclic reduction in oxidative conditions method.[40]

The UV−vis spectra of these clusters give three absorption peaks, one sharp peak at 490 nm and two small peaks at 350 and 650 nm. The intensities of the last two peaks decrease with an increase in the percentage of glutathione, so this study perfectly agrees with the prepared cluster with glutathione of type **3**. In addition, fits for all three clusters are also displayed in this figure. The fit function is a calculated absorption by using the small particle approximation of the Mie theory.[41] Here, the absorption cross section of a spherical particle, which is small compared with the wavelength, can be expressed as follows:

$$\sigma_{abs} = 9\frac{\omega}{c}\varepsilon_m^{3/2}V_0\frac{\varepsilon_2(\omega)}{[\varepsilon_1(\omega) + 2\varepsilon_m]^2 + \varepsilon_2(\omega)^2} \quad (1)$$

V_0 denotes the particle volume and ε_m, the dielectric constant of the surrounding medium. $\varepsilon_1(\omega)$ and $\varepsilon_2(\omega)$ are the real and imaginary parts of the dielectric function, $\varepsilon(\omega)$, of the particle, respectively. The dielectric function of a silver cluster can be derived from the bulk optical constants.[42] To correct $\varepsilon_{bulk}(\omega)$ for particle size and other influences (e.g., the electron spill-out effect), the damping constant of its free electron contribution has to be adapted. This can be done by describing the free electron contribution of $\varepsilon(\omega)$ with the Drude model:[43]

$$\varepsilon(\omega) = \varepsilon_{bulk}(\omega) + \omega_p^2\left(\frac{1}{\omega^2 + \Gamma^2_{bulk}} - \frac{1}{\omega^2 + \Gamma^2_{cluster}}\right) + i\frac{\omega_p^2}{\omega}\left(\frac{\Gamma_{cluster}}{\omega^2 + \Gamma^2_{cluster}} - \frac{\Gamma_{bulk}}{\omega^2 + \Gamma^2_{bulk}}\right) \quad (2)$$

The common textbook value of the plasma frequency for silver, ω_p, is 9.1 eV, and of the bulk damping constant, Γ_{bulk}, it is 0.018 eV. The corrected damping constant of the cluster, $\Gamma_{cluster}$, is one of the fit parameters. The so-derived dielectric function can be inserted in eq 1.

For determining the extinction cross section of the solution, additional scattering losses from the ligands have to be considered, too. The scattering of the cluster can be neglected due to its small size; the ligand molecules, however, can form bigger agglomerates, which act as scattering centers. Here, only Rayleigh scattering is assumed. Consequently, the extinction cross section of the solution is expressed as

$$\sigma_{ext} = \sigma_{abs} + A\cdot\omega^4 \quad (3)$$

The calculation was carried out using eq 3 with the fit parameters A, $\Gamma_{cluster}$, and ε_m. The three fits are in good agreement with the measured data in Figure 7. In Table 1, the extracted values for the three MPCs are listed.

Table 1. Overview of the Values for the Plasmon Peak Position (λ_{max}), the Effective Dielectric Constant of the Surrounding Medium (ε_m), and the Damping Constant of the Plasmon Excitation ($\Gamma_{cluster}$)[a]

MPC	λ_{max} (nm)	ε_m (F·m^{-1})	$\Gamma_{cluster}$ (eV)
Ag@SCH$_2$CH$_2$Ph	464	3.95 ± 0.1	0.9 ± 0.1
Ag@SPhF	461	4.2 ± 0.1	1.1 ± 0.1
Ag@SG	483	4.7 ± 0.1	0.55 ± 0.1

[a]The values are extracted from the fit of the UV-vis spectra of the three cluster samples.

The plasmon resonance of the silver cluster undergoes a strong red shift for all MPCs compared with the vacuum value (from 350 nm to ~470 nm). The reason for this effect is the strong electronic influence of the ligands on the metal core. From formula 1, it can be seen that the plasmon peak is located where the denominator has a minimum. This is the case when $\varepsilon_1(\omega) + 2\varepsilon_m = 0$. Consequently, a change in the electronic environment of the cluster shifts the resonance frequency. In the case of MPCs, the value, ε_m, does not have a direct physical meaning. It can be interpreted as an effective dielectric constant, however. Its value is influenced by properties of the chemical bond such as its strength, polarity, and polarizability.[44] The values of ε_m show big differences between the different MPCs, which suggests different properties of the Ag$_n$-S bonds.

The second derived value is the damping constant of the plasmon. As mentioned in the Introduction, there are mainly two effects that influence its value: cluster size and the electron spill-out that is highly dependent on the electronic properties of the cluster interface. The cluster size cannot be responsible for

dx.doi.org/10.1021/jp210453v | J. Phys. Chem. C 2012, 116, 8034−8043

the observed differences in the measured values because the mean cluster sizes are very similar (see TEM images). The electron spill-out effect, in contrast, should be biggest for ligands, where the electrons of the cluster have to overcome the smallest energy barrier to be transferred to the ligand. This is the case for the $^{-}$SPhF ligand because its large π-electron system is highly polarizable. Consequently, the highest value of the damping constant is found for this MPC (1.1 eV).

Stability of the Silver Monolayer-Protected Clusters (Ag-MPCs). In addition, UV−vis spectroscopy can also be used for the investigation of the stability of the clusters. The samples are usually stored in a fridge at about 0 °C and sealed to avoid exposure to air. Every month, a UV−vis spectrum of the sample was recorded, always using nearly the same concentration (around 1 mg/mL). For all three types of cluster, it was observed that their spectra do not change at all over time (neither the peak positions nor the intensity of the absorbance). Therefore, it can be concluded that all our samples are highly stable at around freezing temperature and in the absence of air.

Silver clusters protected by 2-PET (**1**) are particularly stable, even when being exposed to air. There is no change in the intensity of the absorption peaks of the UV−vis spectra (a characteristic aging pattern) at all, even after 24 h exposure to air (see Figures 8 and S3 (Supporting Information)). In

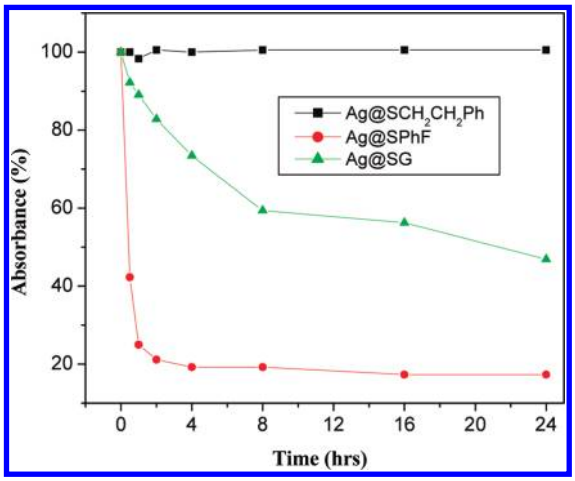

Figure 8. The kinetic study of the stability of nanoclusters (**1**−**3**) in air. The absorbance percentage of cluster **1** stays completely the same over a time period of 24 h, cluster **2** loses half of its absorbance percentage after 30 min, and in cluster **3** the degradation decreases.

contrast to this species, AgNCs protected by 4-FTP (**2**) loose half of their absorbance after 30 min. After that, the absorbance decreases even further, but now, more slowly with time (Figures 8 and S4 (Supporting Information)). A similar behavior can be found for the Ag@SG clusters (**3**): The absorbance decreases slowly with time but not as fast as in the previous case (Figures 8 and S5 (Supporting Information)).

We speculate that the silver-to-sulfur bond is more stable in Ag@SCH_2CH_2Ph than in Ag@SPhF and Ag@SG because the benzyl group is an electron-donating group, and hence, the stability of the Ag−S bond is increased, leading to a higher stability of the clusters of type **1**. In the case of Ag@SG, the carbonyl group is an electron-withdrawing group, and therefore, this effect leads to a lower stability of the Ag−S bond. In the case of 4-fluorothiophenol, the effect is even more pronounced because of the strong electron-withdrawing of the fluoride atom on the aromatic ring.

In addition, the electron spill-out from the clusters to the ligand also supports this assumption: Due to the electron delocalization over the aromatic system, the damping constant is largest at the clusters decorated with 4-fluorothiophenol. In the previous section, we attributed the damping constant to the spill-out effects of the electron density from the cluster to the ligand. This means that the barrier for an electron transfer to the ligand is lowest for Ag@SPhF MPCs because they show the highest damping constant (1.1 eV) of all three clusters. However, in the case of the two other types of clusters (**1** and **2**), the stability and the spill-out is reversed. This shows that the effect of the electron-withdrawing group might probably play a more important role in these cases.

Chirality of the Silver Monolayer-Protected Clusters (Ag-MPCs). During the process of cluster formation, chiral molecules can impart their chiral structure to achiral educts. Therefore, chiral clusters can be formed when they are protected by chiral ligands. The chiral substances show optical activity, which can be obtained using CD spectroscopy. Since the cluster and the ligand show different absorption bands, it can be determined if one or even both species are chiral.[22]

Figure 9 shows the CD spectrum of the used three ligands, 2-PET, 4-FTP, and GSH. As expected, the first two ligands are

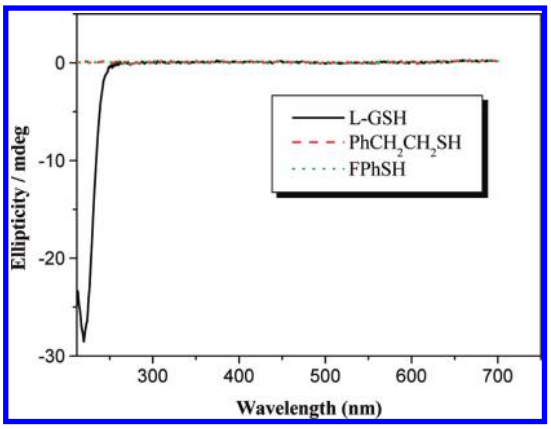

Figure 9. CD spectra of all three ligands used. L-Glutathione is optically active and shows a strong CD signal only at 220 nm. As expected, 2-phenylethanethiol and 4-fluorothiophenol are optically inactive.

optically inactive, but L-GSH shows a strong CD signal at 220 nm. In Figure 10, the CD spectra of all three clusters decorated with different ligands are shown. Although in the case of the clusters that are protected with achiral ligands, no CD effect is visible, clusters that are coated with L-GSH show a CD peak at 281 nm and a second one with lower intensity at 480 nm. Although the peak in the lower wavelength range might be interpreted as the optical transition of the ligand, which is shifted to the red due to the interaction with the cluster, the second peak around 480 nm is a clear indication of metal-based optical activity.[21] The ellipticity of both peaks, however, is very small, which can be attributed to a relatively large distribution of the cluster size. Since for some sizes of clusters, the ellipticity might be negative and in other cases positive, these contributions might average out, leading to a quite small signal. Nevertheless, the effect is clearly visible, and we conclude that in the case of glutathione, the silver nanoclusters

dx.doi.org/10.1021/jp210453v | J. Phys. Chem. C 2012, 116, 8034−8043

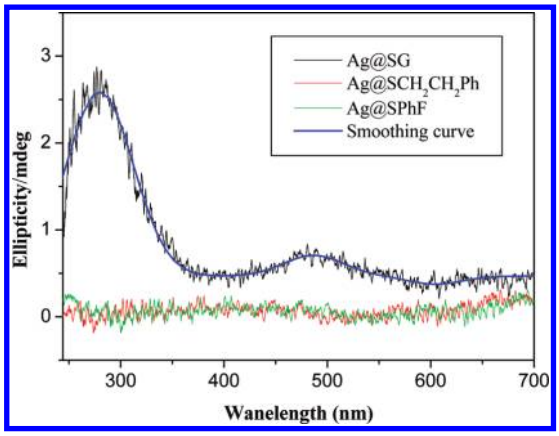

Figure 10. CD spectra of all three ligand-protected silver clusters (**1**−**3**). Ag@SG nanoclusters, which are coated with L-GSH show a strong CD peak at 281 nm and a second one with lower intensity at 480 nm, which is in very good agreement with the work of Cathcart and Kitaev.[40] Because of the nature of the achiral ligand, Ag@SCH$_2$CH$_2$Ph and Ag@SPhF nanoclusters show no optical activity at all.

of type **3** impart the chirality of this specific ligand, thus also becoming chiral.

CONCLUSIONS

We report herein synthesis and characterization of three new silver nanoclusters protected by 2-PET, 4-FTP, and L-GSH ligands. Our results show that spherical silver nanoparticles are produced. The average sizes of the dispersed particles are estimated to be 2.11, 2.7, and 2.08 nm by taking the average 145, 946, and 461 particles for Ag@SCH$_2$CH$_2$Ph, Ag@SPhF, and Ag@SG nanoclusters, respectively. Thermogravimetric analysis and elemental analysis deduce the exact number of silver atoms and thiolate ligands (1/0.75, 1/0.47, and 1/0.76) in the three nanoparticles (**1**−**3**), respectively. The absorption signal of Ag@SCH$_2$CH$_2$Ph in toluene can be found at 469 nm, and Ag@SPhF in THF show two absorption bands at 395 and 462 nm. Ag@SG in water absorbs at 478 nm. Disappearance of the S−H vibrational band (2535−2564 cm^{-1}) in the silver nanoclusters confirms the anchoring of ligands to the cluster surface through the sulfur atom. The spectroscopic measurements by means of UV−vis and FTIR spectroscopy of these clusters revealed that they are molecular in nature and that their optical and photophysical properties are heavily dependent on the ligands, which cover these silver clusters.

ASSOCIATED CONTENT

Supporting Information

FTIR spectra, elemental analysis, atomic absorption spectra, and UV-vis spectra of silver nanoclusters as a function of time at ambient conditions. This material is available free of charge via the Internet at http://pubs.acs.org.

AUTHOR INFORMATION

Corresponding Author

*E-mail: tschurl@tum.de.

Notes

The authors declare no competing financial interest.

ACKNOWLEDGMENTS

This work is supported by an ERC Advanced Grant (ERC-2009-AdG 246645-ASC3) and by the DAAD and Egyptian missions (German Egyptian Research Long Term Scholarship, GERLS). We kindly acknowledge the groups of Prof. Buchner and Prof. Rieger for carrying out the CD and FTIR and TGA measurement, respectively.

REFERENCES

(1) Habibpour, V.; Wang, Z. W.; Palmer, R. E.; Heiz, U. *J. Appl. Sci.* **2011**, *11*, 1164.
(2) Kunz, S.; Schweinberger, F. F.; Habibpour, V.; Rottgen, M.; Harding, C.; Arenz, M.; Heiz, U. *J. Phys. Chem. C* **2010**, *114*, 1651.
(3) Kartouzian, A.; Thaemer, M.; Heiz, U. *Phys. Status Solidi, B* **2010**, *247*, 1147.
(4) Brust, M.; Bethell, D.; Schiffrin, D. J.; Whyman, R. *J. Chem. Soc. Chem. Commun.* **1994**, 801−802.
(5) Gobin, A. M.; Lee, M. H.; Halas, N. J.; James, W. D.; Drezek, R. A.; West, J. L. *Nano Lett.* **2007**, *7*, 1929.
(6) Jain, P. K.; Lee, K. S.; El-Sayed, I. H.; El-Sayed, M. A. *J. Phys. Chem. B* **2006**, *110*, 7238.
(7) Verma, A.; Uzun, O.; Hu, Y. H.; Hu, Y.; Han, H. S.; Watson, N.; Chen, S. L.; Irvine, D. J.; Stellacci, F. *Nat. Mater.* **2008**, *7*, 588.
(8) Haynes, C. L.; McFarland, A. D.; Zhao, L. L.; Van Duyne, R. P.; Schatz, G. C.; Gunnarsson, L.; Prikulis, J.; Kasemo, B.; Kall, M. *J. Phys. Chem. B* **2003**, *107*, 7337.
(9) Park, I.; Ko, S. H.; Pan, H.; Grigoropoulos, C. P.; Pisano, A. P.; Frechet, J. M. J.; Lee, E. S.; Jeong, J. H. *Adv. Mater.* **2008**, *20*, 489.
(10) Sivaramakrishnan, S.; Chia, P. J.; Yeo, Y. C.; Chua, L. L.; Ho, P. K. H. *Nat. Mater.* **2007**, *6*, 149.
(11) Zheng, J.; Nicovich, P. R.; Dickson, R. M. *Annu. Rev. Phys. Chem.* **2007**, *58*, 409.
(12) Aikens, C. M.; Li, S. Z.; Schatz, G. C. *J. Phys. Chem. C* **2008**, *112*, 11272.
(13) Kelly, K. L.; Coronado, E.; Zhao, L. L.; Schatz, G. C. *J. Phys. Chem. B* **2003**, *107*, 668.
(14) Hu, M.; Chen, J. Y.; Li, Z. Y.; Au, L.; Hartland, G. V.; Li, X. D.; Marquez, M.; Xia, Y. N. *Chem. Soc. Rev.* **2006**, *35*, 1084.
(15) Wang, H.; Brandl, D. W.; Nordlander, P.; Halas, N. J. *Acc. Chem. Res.* **2007**, *40*, 53.
(16) Moores, A.; Goettmann, F. *New J. Chem.* **2006**, *30*, 1121.
(17) Kreibig, U; von Fragstein, C. *Z. Phys.* **1969**, *224*, 307.
(18) Zaremba, E; Persson, B. N. J. *Phys. Rev. B* **1987**, *35*, 596.
(19) Harb, M; Rabilloud, F; Félix, C. *J. Chem. Phys.* **2008**, *129*, 194108.
(20) Jadzinsky, P. D.; Calero, G.; Ackerson, C. J.; Bushnell, D. A.; Kornberg, R. D. *Science* **2007**, *318*, 430.
(21) Si, S.; Gautier, C.; Boudon, J.; Taras, R.; Gladiali, S.; Bürgi, T. *J. Phys. Chem. C* **2009**, *113*, 12966.
(22) Slocik, J. M.; Govorov, A. O.; Naik, R. R. *Nano Lett.* **2011**, *11*, 701.
(23) Gautier, C.; Bürgi, T. *ChemPhysChem* **2009**, *10*, 483.
(24) Wu, Z.; Lanni; Chen, E.; Bier, W. M. E.; Ly, D.; Jin, R. *J. Am. Chem. Soc.* **2009**, *131*, 16672.
(25) (a) Schaaff, T. G.; Knight, G.; Shafigullin, M. N.; Borkman, R. F.; Whetten, R. L. *J. Phys. Chem. B* **1998**, *102*, 10643. (b) Wang, Z.; Tan, B.; Hussain, I.; Schaeffer, N.; Wyatt, M. F.; Brust, M.; Cooper, A. I. *Langmuir* **2007**, *23*, 885.
(26) (a) Dass, A.; Stevenson, A.; Dubay, G. R.; Tracy, J. B.; Murray, R. W. *J. Am. Chem. Soc.* **2008**, *130*, 5940. (b) Kim, J.; Lema, K.; Ukaigwe, M.; Lee, D. *Langmuir* **2007**, *23*, 7853. (c) Dass, A. *J. Am. Chem. Soc.* **2009**, *131*, 11666.
(27) (a) Shichibu, Y.; Negishi, Y.; Tsukuda, T.; Teranishi, T. *J. Am. Chem. Soc.* **2005**, *127*, 13464. (b) Negishi, Y.; Chaki, N. K.; Shichibu, Y.; Whetten, R. L.; Tsukuda, T. *J. Am. Chem. Soc.* **2007**, *129*, 11322.
(28) (a) Zhu, M.; Qian, H.; Jin, R. *J. Am. Chem. Soc.* **2009**, *131*, 7220. (b) Qian, H.; Zhu, M.; Andersen, U. N.; Jin, R. *J. Phys. Chem. A* **2009**, *113*, 4281.
(29) Kumar, S.; Bolan, M. D.; Bigioni, T. P. *J. Am. Chem. Soc.* **2010**, *132*, 13141.
(30) Qian, H; Jin, R. *Nano Lett.* **2009**, *9*, 4083.

(31) Chen, S.; Kimura, K. *Langmuir* **1999**, *15*, 1075.
(32) Mohapatra, S.; Mallick, S. K.; Maiti, T. K.; Ghosh, S. K.; Pramanik, P. *Nanotechnol.* **2007**, *18*, 385102.
(33) Chung, C.; Lee, M. *J. Electroanal. Chem.* **1999**, *468*, 91.
(34) Hostetler, M. J.; Stokes, J. J.; Murray, R. W. *Langmuir* **1996**, *12*, 3604.
(35) Yao, H.; Saeki, M.; Kimura, K. *J. Phys. Chem. C* **2010**, *114*, 15909.
(36) Shibu, E. S.; Habeeb Muhammed, M. A.; Tsukuda, T.; Pradeep, T. *J. Phys. Chem. C* **2008**, *112*, 12168.
(37) Tracy, J. B.; Crowe, M. C.; Parker, J. F.; Hampe, O.; Fields-Zinna, C. A; Dass, A.; Murray, R. W. *J. Am. Chem. Soc.* **2007**, *129*, 16209.
(38) Branham, M. R.; Douglas, A. D.; Mills, A. J.; Tracy, J. B.; White, P. S.; Murray, R. W. *Langmuir* **2006**, *22*, 11376.
(39) Ang, T. P.; Chin, W. S. *J. Phys. Chem. B* **2005**, *109*, 22228.
(40) Cathcart, N.; Kitaev, V. *J. Phys. Chem. C* **2010**, *114*, 16010.
(41) Mie, G. *Ann. Phys.* **1908**, *25*, 377.
(42) Johnson, P. B.; Cristy, R. W. *Phys. Rev. B* **1972**, *6*, 4370.
(43) Kreibig, U.; Vollmer, M. *Optical Properties of Metal Clusters*; Springer: Berlin, New York, 1995.
(44) Lica, G. C.; Tong, Y. Y. *J. Phys. Chem.* **2004**, *108*, 19896.